ISSN (Print) 1226-1750
ISSN (Online) 2233-6656
Journal of Magnetics 19(4), 315-322 (2014) http://dx.doi.org/10.4283/JMAG.2014.19.4.315

Concurrent Modeling of Magnetic Field Parameters, Crystalline Structures, and Ferromagnetic Dynamic Critical Behavior Relationships: Mean-Field and Artificial Neural Network Projections

Yongyut Laosiritaworn[1]* and Wimalin Laosiritaworn[2]

[1]*Department of Physics and Materials Science, Faculty of Science, Chiang Mai University, Chiang Mai 50200, Thailand*
[2]*Department of Industrial Engineering, Faculty of Engineering, Chiang Mai University, Chiang Mai 50200, Thailand*

(Received 9 July 2014, Received in final form 12 November 2014, Accepted 17 November 2014)

In this work, Artificial Neural Network (ANN) was used to model the dynamic behavior of ferromagnetic hysteresis derived from performing the mean-field analysis on the Ising model. The effect of field parameters and system structure (via coordination number) on dynamic critical points was elucidated. The Ising magnetization equation was drawn from mean-field picture where the steady hysteresis loops were extracted, and series of the dynamic critical points for constructing dynamic phase-diagram were depicted. From the dynamic critical points, the field parameters and the coordination number were treated as inputs whereas the dynamic critical temperature was considered as the output of the ANN. The input-output datasets were divided into training, validating and testing datasets. The number of neurons in hidden layer was varied in structuring ANN network with highest accuracy. The network was then used to predict dynamic critical points of the untrained input. The predicted and the targeted outputs were found to match well over an extensive range even for systems with different structures and field parameters. This therefore confirms the ANN capabilities and indicates the ANN ability in modeling the ferromagnetic dynamic hysteresis behavior for establishing the dynamic-phase-diagram.

Keywords : artificial neural network, Ising hysteresis, mean-field analysis

1. Introduction

The topic on dynamic hysteresis behavior has long been accepted as a very challenging problem. This is as the dynamic characteristic of the hysteresis is due to the lagging effect between the oscillating driving field and its dependent parameter, e.g. electric field and polarization, magnetic field and magnetization, or mechanical stress and strain. Even at a particular magnitude of the field, there are large number of possibilities that the field at that magnitude can be generated (e.g. by varying starting field, field amplitude, field frequency, and rate of field changing), and this leads to many possibilities the lagging patterns could be. Moreover, the environmental temperature and the microstructure of the investigating materials also have strong effect on the hysteresis. Therefore, the investigation on the hysteresis topic is akin to a going on and on topic. Moreover, apart from fundamental interest, the understanding in hysteresis phenomena is very useful in designing many applications, e.g. transformer, transducer, actuator and digital recording media, etc [1-4]. For instance, magnetic hysteresis with somewhat large coercivity is useful for magnetic recording media in term of data stability, but the hysteresis with fairly low coercivity is required in transformer in minimizing the energy dissipation. As the field features have strong effect on the hysteresis characteristic, field amplitude, field frequency, temperature, and material microstructure dependence of hysteresis parameters are important for enhancing the understanding in the hysteresis topic. Previous experimental and theoretical investigations (e.g. [5-13]) have been previously performed. For instance, the hysteresis area A dependence on the external field parameters (i.e. amplitude h_0, and frequency f) and temperature T were measured and fitted using power law scaling with the $A \propto f^{\alpha} h_0^{\beta} T^{\gamma}$ where α, β and γ are exponents to the scaling [11-13].

However, the success of this power law scaling strongly depends on the range of the fit. Specifically, the hysteresis

*Corresponding author: Tel: +66-86-587-3367
Fax: +66-53-943-445, e-mail: yongyut_laosiritaworn@yahoo.com

area peculiarly varies with the field frequency. With increasing the field frequency, the area increases at low frequencies but decreasing at high frequencies, due to the increase in lagging effect with enhancing the field sweeping magnitude. Therefore, two different scaling forms have to be proposed i.e. power law growth for low frequencies and power law decay for high frequencies, which is inconvenient and fails when the considered frequencies are lying in the region between low and high frequencies. In addition, in some systems, the scaling exponents (α, β and γ) are not constants. For instance, it was found that the frequency exponent (α) can be a function of the field amplitude, and also the amplitude exponent (β) can be a function of field frequencies [13]. Therefore, instead of obtaining simple function being able to predict the hysteresis phenomena, what one gets in this case is a more complicate function.

One description which could be the answer for why the scaling does not work well is that there occurs dynamic phase transition in hysteresis system [9, 14]. The dynamic phase transition is the transition between the dynamic paramagnetic phase (where the hysteresis is a symmetric loop) and the dynamic ferromagnetic phase (where the hysteresis is an asymmetric loop). Similar to the typical static magnetic phase transition, the dynamic transition can be both first order and second order. However, as many parameters, such as the field parameters, the environment temperature, the system structure, influent the lagging phenomena, the dynamic phase transition is more complicated as it also depends on the field frequency (whereas in the static phase transition the frequency is zero) [14, 15]. In addition, the dynamic phase boundaries are quite different between low and high frequencies. Further, it is quite unlikely to find proper formalism being able to describe how the dynamics phase boundaries respond with changing relevant parameter.

Consequently, in this work, we used one of the sophisticate data mining techniques, i.e. the Artificial Neural Network (ANN), in modelling the dynamic hysteresis phase boundaries. This is as the ANN equips with the ability to recognize pattern via 'learning' from experiences. The ANN was occasionally considered in modeling magnetic hysteresis, but those previous works focused only on matching particular simulated Preisach hysteresis shapes with those from experiments [16], or predicting particular sets of hysteresis properties. In addition, although there are previous ANN studies concentrated on the investigation of the change in the hysteresis properties and the finding of relationship among parameters e.g. ferroelectric experiments [17-20], magnetic experiments [21], spin model calculation [22, 23], the use of ANN in establishing the relationship between the dynamic-hysteresis phase-diagrams and important perturbations across systems with different dimension and microstructures is yet to identify. Therefore, the main objective of this work is to provide another step in filling the gap which may be useful for enhancing functional magnetic related devices.

To outline, used as an application, the ferromagnetic Ising model (which represents very strong uniaxial anisotropic magnetic system) was considered. Then, the mean-field analysis, which reduces many body problem into a many single body problems, was used to construct the steady state Ising hysteresis loops. After that, with varying the external field frequency and amplitude, temperature, system structure from one to two dimensions and to bulk system, the dynamic critical points were extracted. The ANN was then performed to relate how dynamic critical points depend on input parameters using multilayer perceptron infrastructure [24, 25]. The ANN modeling was done by varying number of hidden neurons to find the optmized network with highest accuracy. The optimized network was then used to draw dynamic hysteresis phase boundaries, and compared with the real ones. Details of the mean-field and the ANN analysis are given in the next sections, with results detailed in the results and discussion section, where the main finding of the work are summarized and given in the conclusion section.

2. Background Theories and Methodologies

2.1. The Mean-field Extraction of Ising Hysteresis

In this work, the considered system is a ferromagnetic system which its energy can be described using the Ising Hamiltonian i.e.

$$H = -\sum_{\langle ij \rangle} J_{ij} s_i s_j - \sum_i h(t) s_i . \quad (1)$$

In Eq. (1), the spin $s_i = \pm 1$ is the Ising spin, $h(t) = h_0 \sin(2\pi ft)$, f is the field frequency, h_0 is the field amplitude, and t is time. The exchange interaction $J_{ij} = J$ (directional independent), telling how strong is the magnetic interaction between spins, is used as the energy unit, while the spin s_i is considered dimensionless. As a result, unit of temperature T is J/k_B and the unit of the field h is J. The notation $\langle ij \rangle$ specifies that the magnetic interaction range covers only the nearest neighbor pairs. Next, in extracting the hysteresis, mean-field technique was employed. In this mean-field picture, all Ising spins experience the local field generated by the surrounding spins, where the equation of motion for the magnetization m (the spin representative) is given by [26]

Table 1. Example of the coordination number for some crystal structures.

Dimension	Crystal structure	Coordination number (z)
1	Chain	2
2	Square lattice	4
2	Triangular lattice	6
3	Simple cubic	6
3	Body centered cubic	8
3	Face centered cubic	12

$$\tau\frac{dm(t)}{dt} = -m(t) + \tanh\beta\langle E\rangle\,, \tag{2}$$

where $t = 1$ is the spin responding time, β is the inverse temperature i.e. $1/k_{\mathrm{B}}T$, k_B is the Boltzmann constant, and $\langle E\rangle$ is the local field. By setting $\tau = 1$ and used as the unit of time, $\beta\langle E\rangle$ is given by

$$\beta\langle E\rangle = \frac{zJm(t) + h(t)}{k_BT}\,. \tag{3}$$

In Eq. (3), z refers to number of nearest neighboring which in lattice language z is the coordination number. As spins locate on atomic lattice sites in solid magnetic materials, different z then refers different crystal structure. Example of z and its associated system is given in Table 1.

To extract the magnetization m as a function of time t, the mean-field Eq. (2) was solved using the fourth order Runge-Kutta method [27]. To draw a hysteresis loop, at least 1000 data point was found to compromise between calculation time required and quality of the hysteresis loop shape. Therefore, the time step for solving the differential Eq. (2) is $\Delta t = P/1000$ where P is the period of the external magnetic field. Next by setting initial magnetization as $m(0) = 1.0$, the fourth order Runge-Kutta (RK) was performed to draw the hysteresis loops (the m-h relation). In each loop, the dynamic order parameter $Q = \frac{1}{\text{period}}\int^{\text{period}} m(t)dt$ (the period average magnetization) was used to judge if the hysteresis has asymmetric shape ($Q \neq 0$) or symmetric shape ($Q = 0$). Then, the RK procedure was repeated until the hysteresis loop arrives at its steady state. This steady state condition can be checked by the convergence of Q. For instance, whenever the difference in Q between consecutive loops (i.e. ΔQ) is zero, the system is now residing in its steady state and Q is now applicable for indicating if the hysteresis has symmetric shape (dynamic paramagnetic behavior) or asymmetric shape (dynamic ferromagnetic behavior). However, it is still not trivial to exactly locate the steady state using this method because of the numerical rounding error in computer. Further, the calculation time (human time) required to reach steady state is very lengthy at high frequencies. Consequently, the criteria $\Delta Q = 10^{-5}$ was used to be the representative of 'zero Q' [14]. Smaller ΔQ do not significantly change dynamic phase boundary results. In this work, both the temperature (T) and field amplitude were ranged from 0.025 to 12.0 J/k_B, the field frequency (f) was ranged from 0.001 to 3.000 τ^{-1}, and the coordination number z in the set {2,4,6,8,12} was used.

Note that, these parameters and their ranges were fed into the Artificial Neural Network for artificial-intelligent modeling. The input parameters to the network were the coordination numbers (representing the system structural characteristic) as well as the field frequencies and amplitudes (representing the rate and strength of the external field perturbation), where the output parameter was the temperatures T at the dynamical critical boundaries. This so called dynamic critical temperature T is important to specify the dynamic hysteresis behavior of the ferromagnetic system. For temperatures larger than this critical T, the hysteresis loop has symmetric shape whereas for temperatures lower than this critical T, the hysteresis loop has asymmetric shape. As can be seen, this dynamic critical temperature T is crucial in the fundamental understating of hysteresis phenomena which suggest the range of operating conditions for magnetic application for avoiding the undesired asymmetric hysteresis properties. Therefore, the dynamic critical temperature T was chosen as the important output to be modeled by the Artificial Neural Network.

2.2. Artificial Neural Network

The Artificial Neural Network (ANN) is a data mining technique which mimics how the human brain functions in recognizing patterns via experiencing and learning. Therefore, it can be used to establish connections among inputs and outputs of the considered datasets. In brief, the ANN consists of many processing elements (called neurons), connected together. In multilayer perceptron infrastructure [24, 25], neurons reside in input layer, hidden layers and the output layer. Then ANN in trained to realize relationship by varying weights or the strength of the connection among pairs of neurons. During the training, sets of input-output data are fed to the network while the weights are adjusted to minimize the error between the predicted outputs and the desired outputs (targets). Once the error becomes minimal, the network is successfully trained and can now be used to predict outputs for any unseen inputs.

In general, the weight is adjusted using some learning algorithms, where in this work, the Back Propagation (BP) learning algorithm [28] was used in the training. The BP learning algorithm can be described as the following [24]. Firstly, inputs are supplied to the neurons in the

input layer. Then, the weighted sum $S_j = \sum_i k_i w_{ij}$, calculated from all neural i in the current layer, is prepared for the neuron j in the next layer. In the sum, k_i is the input to the neuron i, and w_{ij} is the weight from neural i to neural j. After that, the sigmoid transfer function, i.e. $g(x) = \frac{1}{1+e^{-x}}$ where $x = S_j$, is applied on the sum S_j. This $g(x = S_j)$ then becomes the output of neuron i or the input to neuron j. This procedure repeats for all neuron-neuron connections in both input and hidden layers. After that, an error is calculated to adjust the weight for each neuron. For the output layer, the error takes the form $\delta_j = (t_j - a_j)g'(S_j)$ while in the hidden layer the error takes the form $\delta_j = \left[\sum_i \delta_k w_{kj}\right] g'(S_j)$. In these equations, t_j is the target value for neuron j, a_j is the output value for neuron j, $g'(x)$ is the first-order derivative of the g, S_j is weighted sum of inputs to neuron j, and the weight adjustment is calculated from $\Delta w_{ji} = \eta \delta_j a_i$ where η is the learning rate. All these processes get repeated with new input sets until stopping criteria are met.

3. Results and Discussions

With vary the field parameters (i.e. f, h_0), the temperature T and the coordination number z, intriguing hysteresis behavior has been found as shown in Fig. 1. In the figure, the hysteresis dependence on the input perturbation is rather strong. With increasing z and f in Fig. 1(a, b), the hysteresis loops change from symmetric to asymmetric behavior. This is expected as the increase in z yields stronger ferromagnetic interaction per spin (as there are more nearest neighboring) while the increase in f means the increase of field sweeping rate per period. These two cases obviously enhance the lagging effect so less symmetric behavior is the result.

On the other hand, with increasing the field amplitude h_0 and the environment temperature T in Fig. 1(c, d), the

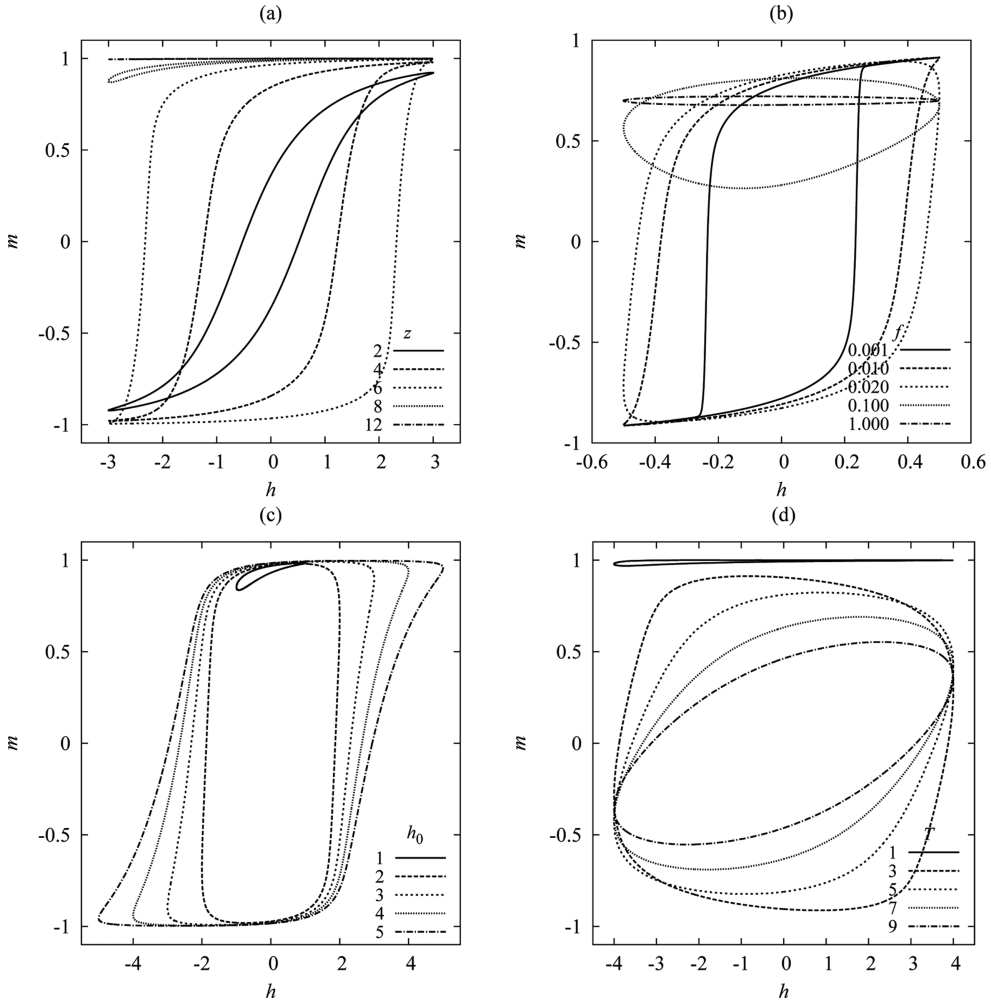

Fig. 1. The Ising hysteresis loops (m-h relationship) obtained from solving Eq. (1) via the mean-field analysis with varying (a) coordination number z, (b) field frequency f, field amplitude h_0 and (d) temperature T. In (a) $f = 0.01\ \tau^{-1}$, $h_0 = 3\ J$ and $T = 3\ J/k_B$. In (b) $z = 2$, $h_0 = 0.5\ J$ and $T = 1.5\ J/k_B$. In (c) $z = 4$, $f = 0.03\ \tau^{-1}$, $T = 2\ J/k_B$. In (d) $z = 12$, $f = 0.07\ \tau^{-1}$ and $h_0 = 4\ J$.

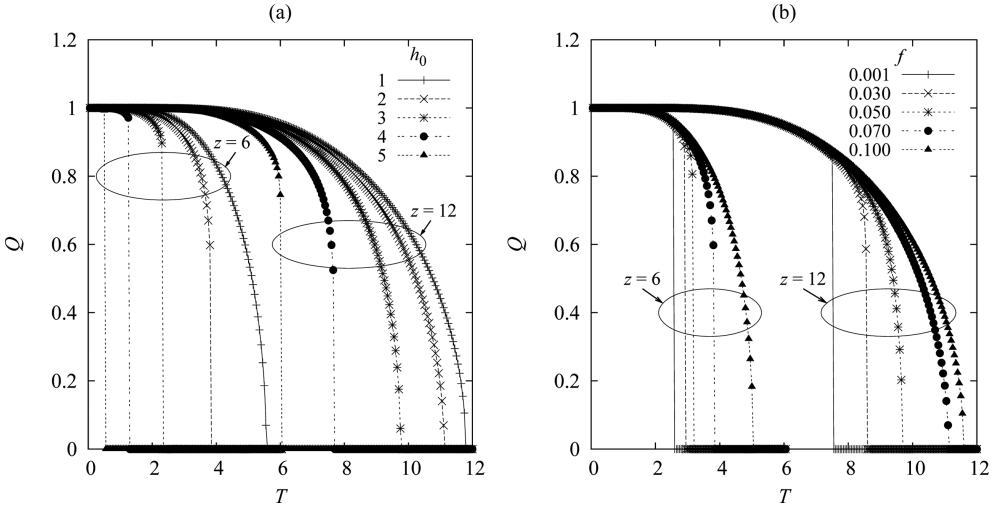

Fig. 2. The period average magnetization Q as a function of temperature T with varying (a) field amplitude h_0 and (b) field frequency f for $z = 6$ and 12 systems. In (a) f was fixed at 0.01 τ^{-1} and in (b) h_0 was fixed at 2 J.

hysteresis loops change from asymmetric to symmetric behavior. This is as on increasing the amplitude implies supplying more magnetic driving force into the system, while the increase in T enhances thermal fluctuation among spins which compensates the spin interaction. These two h_0 and T contributions then allow the spin more mobility to follow the field changing so the lagging effect reduces. Therefore, the symmetric behavior becomes more prominent on increasing h_0 and T. These results are in good agreement with previous applicable investigations [9, 14].

With a focus on the symmetric and asymmetric behavior of the hysteresis loops, the period average magnetization Q was investigated in details. Example of the Q results can be shown as in Fig. 2 where in Fig. 2(a) the amplitude h_0 was varied, but in Fig. 2(b) the frequency f was varied. As can be seen, the dynamic hysteresis phase transition temperature (the lowest temperature that gives 'zero' Q) shifts to higher temperature with increasing f and z, but with reducing h_0. These results agree well with the results in Fig. 1 where the lagging phenomenon is the reason behind.

Next, by recording the dynamic transition temperature T for various f, h_0 and z, the dynamic hysteresis phase-diagram can be defined. Example of the diagram for $z = 6$ can be shown as in Fig. 3. In the figure, there exist boundary lines where each line consists of the dynamic phase boundary data collected from a same field frequency f. The line was drawn using cubic-spline interpolation, where the region below the line refers to sets of (T, h_0) that gives asymmetric hysteresis loops (dynamic ferromagnetic phase) but those above the line gives symmetric hysteresis loops (dynamic paramagnetic phase). Also, the boundary lines move upwards with increasing the frequency f as more thermodynamic energy or magnetic work are required to overcome the increase of lagging effect due to higher field sweeping rate. However, formulating some function that could relate T, h_0, and f on the dynamic boundaries is not trivial as each dynamic boundary has

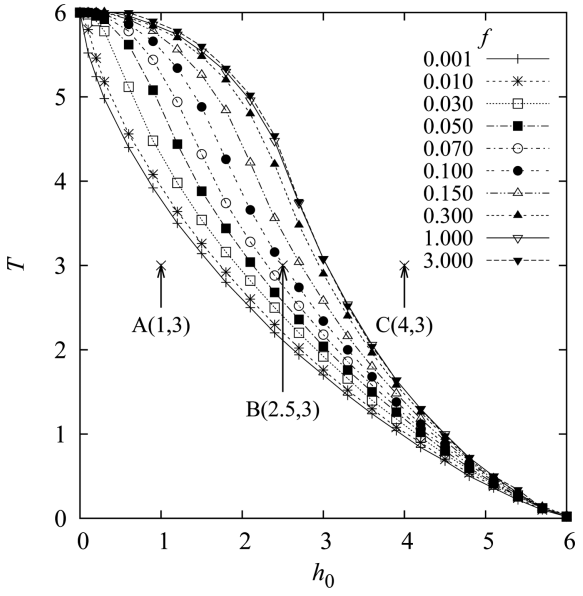

Fig. 3. The dynamic hysteresis phase-diagram for $z = 6$ Ising hysteresis loops. Each line (drawn by using cubic spline interpolation) in the figure links the phase boundary data extracted from different field frequency. Sets of (h_0, T) below a particular curly line belong to the dynamic ferromagnetic phase while those above the line belong to the dynamic paramagnetic phase. Specifically, points A and C are examples of (T, h_0) that are in dynamic ferromagnetic and dynamic paramagnetic phases (for all considered frequencies), respectively, where are point B resides in either ferro- or para-phases depending on the considered frequencies.

Table 2. The range of input and output data used in the ANN training.

Symbol	Description	Type	Input or output	Actual range	Scaling range	Scaling factor
z	Coordination number (number of nearest neighbor spins)	Category	Input	2, 4, 6, 8, and 12	N/A	N/A
$\log_{10}(f)$	Logarithmic frequency (base 10)	Numeric	Input	–3 to 0.477121	[–1, 1]	0.575188
$\log_{10}(h_0)$	Logarithmic amplitude (base 10)	Numeric	Input	–1.60206 to 1.07918	[–1, 1]	0.745923
$\log_{10}(T)$	Logarithmic temperature (base 10)	Numeric	Output	–2 to 1.08063	[0,1]	0.324609

different characteristic and strongly depend on the range of f. Furthermore, although different z share the same qualitative results (similar trends), the quantitative results are somewhat different, i.e. the enhanced level of h_0 and T. Therefore, this even brings more complication into the scaling. Consequently, the ANN was introduced to fill this scaling gap.

However, before starting the ANN procedure, data verifying and cleansing is typically a first step to do to maximize the best use of the ANN modeling. With careful attention on the provided data, it was found that there is somewhat low number of data contributed to the unusual pattern of data. For instance, considering data for $f = 1.0$ and 3.0 τ^{-1} in Fig. 3, unusual trend was found on increasing h_0 i.e. the drop of T is rather slow at low h_0, become great at intermediate h_0 and change to a slow drop again at high h_0. In addition, the range of f is not uniformly distributed but rather increases in an exponential pattern. Therefore, there are some regions of the parameters that the ANN will have less experiences so the ANN may not function well over the whole considered range. As a result, the input-output data were considered in logarithmic scale to allow the more uniformity of the data distribution, and then scaled into the same range. In addition, since z is indeed a discrete variable where different z refers different structure, therefore z was treated as a category type. Details of the data cleansing and categorizing is shown in Table 2.

After all data have been scaled, the inputs (which are z, h_0 and f) and output (which is T) were fed to the ANN. The number of hidden layers and nodes were varied to obtain the network with highest accuracy. The search was carried out for up to 2 hidden layers and up to 40 nodes in each hidden layer. The results of best network are 7:38:14:1. Note that the network was displayed as 4 numbers which indicate number of neurons in input, first hidden, second hidden, and output layers, respectively. Schematic diagram showing the used ANN network can be found in Fig. 4.

In ANN training process, dataset were separated into training, validating, and testing datasets at the ratios 0.6, 0.16, and 0.16 respectively. Note that the training datasets were used to train the network, validating datasets were used to prevent overtraining, and testing datasets were used to test the network accuracy. In this work, 1100 datasets were separated to 748, 176, and 176 datasets, where the ANN accuracy was judged from mean absolute error (MAE) and the coefficient of determination (R^2; R-square) i.e.

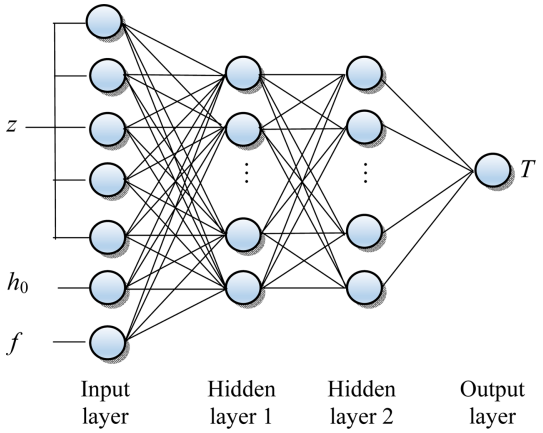

Fig. 4. (Color online) The schematic diagram of the ANN network.

$$\text{MAE} = \frac{\Sigma_{i=1}^{n}|f_i - y_i|}{n} \text{ and}$$

$$R = \frac{n\Sigma_{i=1}^{n} f_i y_i - (\Sigma_{i=1}^{n} f_i)(\Sigma_{i=1}^{n} y_i)}{\sqrt{n(\Sigma_{i=1}^{n} f_i^2) - (\Sigma_{i=1}^{n} f_i)^2}\sqrt{n(\Sigma_{i=1}^{n} y_i^2) - (\Sigma_{i=1}^{n} y_i)^2}}. \quad (4)$$

In Eq. (4), f_i is the ANN predicted output, y_i is the actual target, and n is the total number of dataset used. Note that the lower of the MAE and the closer of the R^2 to 1 are preferable to guarantee the accuracy of the network. The results for both MAE and R^2 are presented in Table 3. As can be seen, the MAE obtained is low, e.g. 0.0226 from the testing data. In addition, $R^2 = 0.9954$ for the testing data is very close to 1. This indicates that the proposed ANN model is reliable. For a visual presentation, the target and the ANN predicted outputs were plotted and compared as shown in Fig. 5. As can be seen, both outputs match very as the scattering plot between the predicted and target outputs almost fall into a linear line

Table 3. ANN training and testing results from the networks 7:38:14:1.

ANN Output	Training		Validating		Testing		Overall (average)	
	MAE	R^2	MAE	R^2	MAE	R^2	MAE	R^2
T	0.0193	0.9974	0.0235	0.9951	0.0226	0.9954	0.0205	0.9968

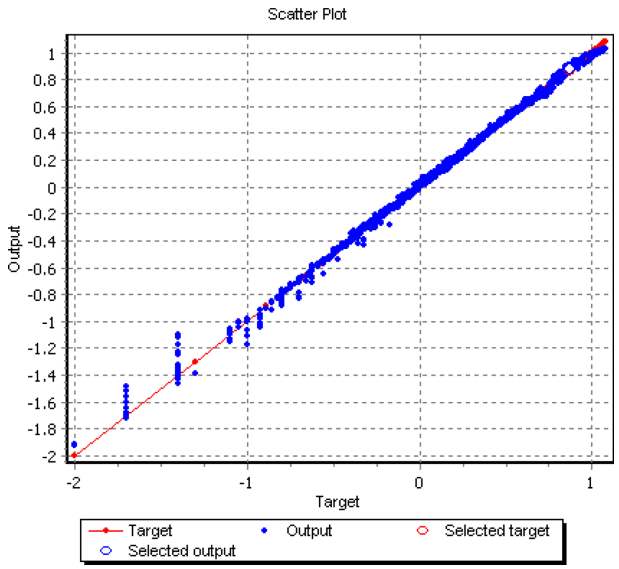

Fig. 5. (Color online) The target output versus predicted output scattering plot for parameter Q from the ANN modeling, using all data from training, validating and testing dataset. The straight line is from linear fit between ANN output and the actual target having $R^2 > 0.9968$ which implies the high accuracy of the ANN modeling.

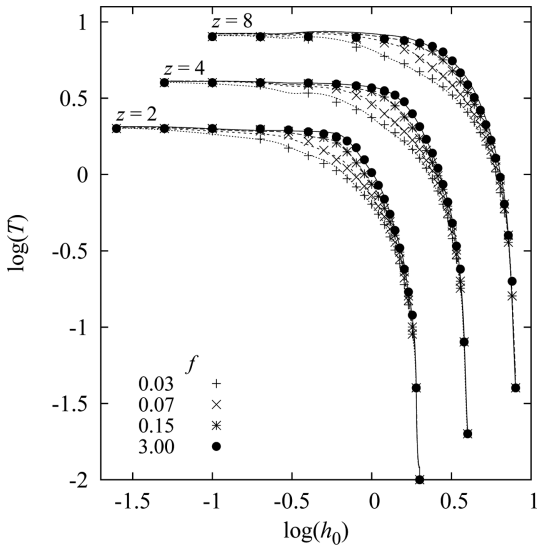

Fig. 6. Example of the comparison of the ANN predicted output and the target (actual) output for $z = 2$, 4 and 8 systems. The data points are from the actual hysteresis results, while curves are drawn from ANN predicted results.

with $R^2 > 0.9968$.

To compare the predicted results on the dynamic phase-diagram, the ANN prediction of the phase-boundaries were drawn and shown in Fig. 6. The discrete data points in the figure are from the target output while curves passing data points are from ANN prediction. As is seen, good agreement is found even using data from different systems (different z) in modeling altogether. This therefore indicates the high accuracy of the constructed ANN model in predicting dynamic phase-diagram of the hysteresis phenomena. This work therefore shows the success of using the ANN in modeling ferromagnetic hysteresis over an extensive range of magnetic field parameters even from different crystalline structures.

4. Conclusion

In this work, the Artificial Neural Network was used to model dynamic hysteresis phenomena especially its dynamic critical behavior using hysteresis data derived from mean-field extraction of the Ising magnetization equation of motion. The Neural Network was trained to relate the coordination number of the system, the field amplitude and the field frequency, to the dynamic critical temperature (i.e. the dynamic phase boundary reconstruction). From the Neural Network training, the best network was achieved and used to generate the predicting output in benchmarking with the real target output. From the scrutinizing, outputs were found to agree well over the extensive range of considered parameters. Therefore, this work illustrates the validities of using the Artificial Neural Network in concurrent modeling dynamic ferromagnetic phase transition phenomena with diverse crystalline structures.

References

[1] M. E. Lines and A. M. Glass, Principles and Applications of Ferroelectrics and Related Materials, Clarendon Press, Oxford (1997).
[2] J. F. Scott, Ferroelectric Memories, Springer-Verlag, Berlin (2002).
[3] A. Moser, K. Takano, D. T. Margulies, M. Albrecht, Y. Sonobe, Y. Ikeda, S. H. Sun, and E. E. Fullerton, J. Phys. D-Appl. Phys. **35**, R157 (2002).
[4] M. L. Plumer, J. v. Ek, and D. Weller, The Physics of

Ultra-High-Density Magnetic Recording, Springer-Verlag, Berlin (2001).
[5] J.-S. Suen, M. H. Lee, G. Teeter, and J. L. Erskine, Phys. Rev. B **59**, 4249 (1999).
[6] W. Y. Lee, B. C. Choi, Y. B. Xu, and J. A. C. Bland, Phys. Rev. B **60**, 10216 (1999).
[7] W. Y. Lee, A. Samad, T. A. Moore, J. A. C. Bland, and B. C. Choi, Phys. Rev. B **61**, 6811 (2000).
[8] M. Acharyya and B. K. Chakrabarti, Phys. Rev. B **52**, 6550 (1995).
[9] B. K. Chakrabarti and M. Acharyya, Rev. Mod. Phys. **71**, 847 (1999).
[10] C. N. Luse and A. Zangwill, Phys. Rev. E **50**, 224 (1994).
[11] R. Yimnirun, A. Ngamjarurojana, R. Wongmaneerung, S. Wongsaenmai, S. Ananta, and Y. Laosiritaworn, Appl. Phys. A **89**, 737 (2007).
[12] R. Yimnirun, R. Wongmaneerung, S. Wongsaenmai, A. Ngamjarurojana, S. Ananta, and Y. Laosiritaworn, Appl. Phys. Lett. **90**, 112906 (2007).
[13] N. Wongdamnern, A. Ngamjarurojana, Y. Laosiritaworn, S. Ananta, and R. Yimnirun, J. Appl. Phys. **105**, 044109 (2009).
[14] A. Punya, R. Yimnirun, P. Laoratanakul, and Y. Laosiritaworn, Physica B **405**, 3482 (2010).
[15] Y. Laosiritaworn, K. Kanchiang, and R. Yimnirun, Ferroelectrics **425**, 72 (2011).
[16] C. Serpico and C. Visone, IEEE Trans. Magn. **34**, 623 (1998).
[17] W. Laosiritaworn, R. Yimnirun, and Y. Laosiritaworn, Key Eng. Mat. **421**, 432 (2010).
[18] W. Laosiritaworn, A. Ngamjarurojana, R. Yimnirun, and Y. Laosiritaworn, Ferroelectrics **401**, 233 (2010).
[19] W. Laosiritaworn, N. Wongdamnern, R. Yimnirun, and Y. Laosiritaworn, Ferroelectrics **414**, 90 (2011).
[20] W. Laosiritaworn, S. Wongsaenmai, R. Yimnirun, and Y. Laosiritaworn, Int. J. Phys. Sci. **6**, 5996 (2011).
[21] J. Faiz and S. Saffari, Electromagnetics **30**, 376 (2010).
[22] W. Laosiritaworn and Y. Laosiritaworn, IEEE Trans. Magn. **45**, 2644, 4957795 (2009).
[23] W. Laosiritaworn and Y. Laosiritaworn, Polyhedron **66**, 108 (2013).
[24] J. E. Dayhoff, Neural Network Architectures: An Introduction, Van Nostrand Reinhold, New York (1990).
[25] K. Swingler, Applying Neural Networks: A Practical Guide, Academic Press, London (1996).
[26] M. Suzuki and R. Kubo, J. Phys. Soc. Jpn. **24**, 51 (1968).
[27] W. H. Press, B. P. Flannery, S. A. Teukolsky, and W. T. Vetterling, Numerical Recipes in C: The Art of Scientific Computing, Cambridge University Press, Cambridge (1992), 2nd edn.
[28] C. A. O. Nascimento, R. Giudici, and R. Guardani, Comput. Chem. Eng. **24**, 2303 (2000).